Immunity
Article

Immobilized Chemokine Fields and Soluble Chemokine Gradients Cooperatively Shape Migration Patterns of Dendritic Cells

Kathrin Schumann,[1,8] Tim Lämmermann,[1,8] Markus Bruckner,[2] Daniel F. Legler,[2] Julien Polleux,[3] Joachim P. Spatz,[3] Gerold Schuler,[4] Reinhold Förster,[5] Manfred B. Lutz,[6] Lydia Sorokin,[7] and Michael Sixt[1,*]
[1]Hofschneider Group Leukocyte Migration, Max Planck Institute of Biochemistry, 82152 Martinsried, Germany
[2]Biotechnology Institute Thurgau at the University of Konstanz, CH-8280 Kreuzlingen, Switzerland
[3]Department of New Materials and Biosystems, Max Planck Institute of Metal Reserach, 70569 Stuttgart, Germany
[4]Department of Dermatology, University Hospital Erlangen, 91052 Erlangen, Germany
[5]Institute of Immunology, Hannover Medical School, 30625 Hannover, Germany
[6]Institute for Virology and Immunobiology, University of Würzburg, 97078 Würzburg, Germany
[7]Institute for Physiological Chemistry and Pathobiochemistry, University of Münster, 48149 Münster, Germany
[8]These authors contributed equally to this work
*Correspondence: sixt@biochem.mpg.de
DOI 10.1016/j.immuni.2010.04.017

SUMMARY

Chemokines orchestrate immune cell trafficking by eliciting either directed or random migration and by activating integrins in order to induce cell adhesion. Analyzing dendritic cell (DC) migration, we showed that these distinct cellular responses depended on the mode of chemokine presentation within tissues. The surface-immobilized form of the chemokine CCL21, the heparan sulfate-anchoring ligand of the CC-chemokine receptor 7 (CCR7), caused random movement of DCs that was confined to the chemokine-presenting surface because it triggered integrin-mediated adhesion. Upon direct contact with CCL21, DCs truncated the anchoring residues of CCL21, thereby releasing it from the solid phase. Soluble CCL21 functionally resembles the second CCR7 ligand, CCL19, which lacks anchoring residues and forms soluble gradients. Both soluble CCR7 ligands triggered chemotactic movement, but not surface adhesion. Adhesive random migration and directional steering cooperate to produce dynamic but spatially restricted locomotion patterns closely resembling the cellular dynamics observed in secondary lymphoid organs.

INTRODUCTION

Chemokines are central orchestrators of the hematopoietic system. They control leukocyte migration and positioning within tissues and direct recirculation patterns by inducing extra- or intravasation at vascular sites. On the cellular level, two main responses are triggered upon chemokine receptor signaling: (1) integrin activation that causes adhesion to endothelial surfaces and (2) polarization of the actomyosin cytoskeleton that causes migration along chemokine gradients (Rot and von Andrian, 2004).

Surface adhesion and migration are traditionally viewed as interdependent phenomena, and in mesenchymal and epithelial cells, the integrin repertoire of a cell restricts its migratory ability to defined tissue environments (Vicente-Manzanares et al., 2009). Adhesive migration is termed *haptokinesis* when migration is random or *haptotaxis* when cells move along concentration gradients of immobilized ligands (Friedl et al., 2001). Haptic movement is strictly confined to an adhesive surface or track as the immobilized integrin ligands play dual roles as mechanical anchors and instructive signals. Leukocytes employ fundamentally different modes of migration, and recent studies have demonstrated that within three-dimensional (3D) environments such as the interstitium, they can directly convert actomyosin forces into locomotion without utilizing integrin-mediated force coupling. Hence, in leukocytes, adhesion and migration can occur independently (Friedl et al., 1998; Lämmermann et al., 2008; Woolf et al., 2007). We have previously shown that adhesion-independent movement can be triggered by soluble chemokines, resulting in *chemokinesis* (random migration) in response to homogenous chemokine signals or *chemotaxis* (directed migration) when cells migrate along soluble chemokine gradients (Lämmermann et al., 2008, 2009).

As chemokines can induce both integrin activation and polarization of the cytoskeleton, the question arises: what determines whether only one or both responses are triggered, i.e., when does a chemokine induce leukocytes to adhere, migrate, or adhere and migrate?

The best-investigated chemokine effect is the triggering of integrin inside-out signaling, which mediates tight adhesion of leukocytes to the endothelium during extravasation from the bloodstream (Ley et al., 2007). It is well established that at sites of inflammation, chemokines are immobilized to the vascular lumen via cell-anchored sugar residues or scavenger receptors (Middleton et al., 1997; Pruenster et al., 2009; Rot and von Andrian, 2004). This immobilization appears to be a prerequisite for inducing leukocyte surface adhesion, and there is evidence

that soluble chemokines do not efficiently trigger adhesion (Shamri et al., 2005). This suggests that the mode of chemokine presentation might determine the cellular response. If and how the presentation form of a chemokine affects leukocyte migration has not been systematically investigated. It is also not known how chemokines are presented within tissues. In principle, they could form homogenous fields or spatial gradients and could either be freely diffusible or immobilize to cellular or extracellular surfaces (Miyasaka and Tanaka, 2004).

In this study, we investigate how chemokine presentation within tissues can shape the leukocytes' chemokinetic, haptokinetic, chemotactic, and haptotactic responses. As a model system, we use dendritic cells (DCs), antigen-presenting cells that sample the periphery and, upon exposure to infection or inflammatory stimuli, migrate into the draining lymph node where they present peripherally acquired antigens to naive T cells (Alvarez et al., 2008; Mellman and Steinman, 2001). DC migration to the lymph node is entirely dependent on the CC-chemokine receptor 7 (CCR7), which is upregulated after pathogen contact (Förster et al., 1999; Ohl et al., 2004; Sallusto et al., 1998) and recognizes two ligands, CCL19 and CCL21. CCL21 is expressed on afferent lymphatic vessels and guides DCs into the vessel lumen, while within the lymph node, CCL21 is produced by fibroblastic reticular cells (FRCs), the stromal cells of the T cell area (Luther et al., 2000). FRCs also express CCL19, albeit in much smaller amounts (Luther et al., 2002). Apart from mature DCs, naive T cells and activated B cells express CCR7, and CCL19 as well as CCL21 are the decisive homeostatic chemokines that direct these cell types into a common compartment of the lymph node where they interact (Junt et al., 2004; Reif et al., 2002). Why are there two chemokines for the same receptor? While equal receptor binding potency suggests redundancy (Kohout et al., 2004), both chemokines differ in their ability to bind to heparan sulfate residues. This difference is because of a highly charged 40 amino acid extension at the C terminus of CCL21 that is lacking in CCL19. It has been shown that this region immobilizes CCL21 while CCL19 is largely soluble (de Paz et al., 2007; Hirose et al., 2002; Patel et al., 2001). In vivo, C-terminal truncation of CCL21 prevents its immobilization to the lumen of high endothelial venules and consequently abolishes its ability to trigger lymphocyte extravasation (Stein et al., 2000).

Here, we show that CCL21 immobilized on FRCs creates a haptokinetic surface for DCs because it triggers both integrin-dependent adhesion and motility. We show that haptokinesis on immobilized CCL21 can be directionally biased by gradients of soluble CCL21 or CCL19, which alone trigger directed migration, but not adhesion. This principle combines the robustness of a haptokinetic surface with the flexibility of a chemotactic gradient. The result is locally adjustable leukocyte swarming within confined areas as it is found in lymphatic organs.

RESULTS

A Reductionist In Vitro System to Study Chemokine-Driven DC Migration

The abundant chemokine in the T cell area of lymph nodes is CCL21 as detected by immunohistology on cryosections (Luther et al., 2000; Woolf et al., 2007). As mature DCs migrate vigorously in response to CCR7 ligands, we tested whether DCs could be employed as environmental sensors of chemokine distribution on cryosections. We layered mature bone marrow-derived DCs on unfixed cryosections of inguinal mouse lymph nodes and followed their behavior by time-lapse video microscopy. In this setup, the cells showed a highly synchronized wave of directed migration from the periphery toward the inner part of the lymph node section (Figures 1A–1C; Movie S1 available online). Twelve to eighteen hours after the onset of migration, DCs accumulated in the center of the lymph node. Migration was observed only when mature DCs were employed and not immature DCs (Figure 1B) or other cell types, including macrophages, mast cells, B cells, and T cells (data not shown).

As migratory activity was restricted to defined areas, we tested whether these areas represented the physiological entry routes and combined in vivo and in vitro migration assays to address this issue. Mice were injected subcutaneously with fluorescently labeled mature DCs, and draining lymph nodes were excised after 10 hr. Costaining of the stromal backbone showed that the transferred DCs located to the interfollicular areas (Figure 1D, left panel). Consecutive sections were then used as substrates for in vitro assays. Single-cell tracking of DCs revealed migrating cells in areas that also contained the DCs that had migrated in vivo (Figure 1D, right panel).

Response Patterns to CCL21

To define the extracellular signals directing the cells, we employed mature *Ccr7*$^{-/-}$ DCs in the cryosection assays and found no accumulation in the center of the section (Figure 2A). Similarly, mature wild-type (WT) DCs did not accumulate on lymph node sections obtained from *plt/plt* mice, which lack expression of both CCR7 ligands (Nakano et al., 1998), while *plt/plt* DCs accumulated on WT sections (Figure 2A). These findings suggest that CCR7 present on the DCs and CCR7 ligands present on the sections are essential for DC migration on lymph node sections. We conclude that DC migration on cryosections recapitulates the physiological process, while complex intercellular crosstalks are largely excluded as the section is not alive.

A simple explanation for the directional movement of the DCs was migration along a graded distribution of CCR7 ligand that is immobilized on the section. In order to visualize immobilized gradients, we immunostained for CCL21 and CCL19. In accordance with previous studies (Luther et al., 2000), CCL19 was not detectable with our histological techniques, while CCL21 signal decorated the reticular network of the T cell parenchyma and left B cell follicles unstained (Figure 2B). Consistent with a previous report (Okada and Cyster, 2007), the gross staining pattern suggested concentration of CCL21 in the center of the lymph node.

To investigate the possibility of DC migration along an immobilized CCL21 gradient, a peripheral portion of a lymph node cryosection was removed and repositioned at 180° to the remaining tissue section (Figure 2C, left panel). Here, DCs showed a wave of directed migration, with migration on the inverted tissue segment still being directed toward the center of the larger segment (Figure 2C, right panel; Movie S2). Migration ceased at the margin of the section as DCs migrate poorly on glass surfaces. Hence, on the inverted segment, the migration direction had changed relative to the tissue substrate. These

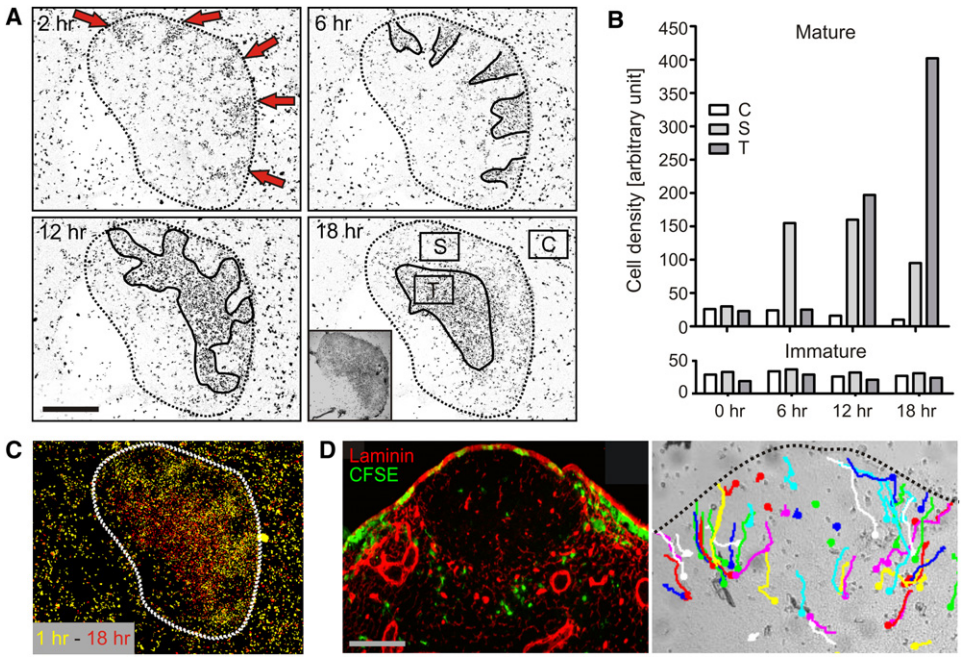

Figure 1. Organized Dendritic Cell Migration on Lymph Node Cryosections

(A) Contrast enhanced serial images of mature dendritic cells (DCs) on a section. Margins of the section are highlighted by the dotted line. Areas of high DC density are outlined (black line). Red arrows indicate entry sites of DCs. Small insert: brightfield image of the lymph node (LN) cryosection. Black boxes mark T cell area (T), sinus area (S), and control area (C) used for quantification in (B). Scale bar represents 200 μm.

(B) DCs were quantified in the areas C, S, and T by automated density measurement. The upper diagram represents mature; the lower represents immature DCs. Data represent one out of > 30 independent experiments.

(C) Composite picture of serial images of (A). Different time points were colorized in graded wavelengths from yellow (1 hr) to red (18 hr) to show migratory fractions of DCs on the section. Dotted line: outline of the section.

(D) Left panel: section of a lymph node showing fluorescently labeled DCs (green) entering the lymph node via interfollicular areas 10 hr after subcutaneous injection. Laminin staining (red) highlights the reticular fibers surrounding the B cell follicle. Right panel: single-cell tracking of DCs migrating on a consecutive section of the one shown left. Each track represents the pathway of a single cell. Dotted line: outline of the section. Scale bar represents 50 μm.

results disprove migration along an immobilized gradient and suggest the involvement of a soluble gradient, originating from the T cell area.

To reduce the complexity of our assays, we next investigated migration in response to immobilized CCL21. DCs were followed by video microscopy while being exposed to a cell culture polystyrene surface decorated with a spot of immobilized CCL21. DCs directly settling onto the coated area showed rapid spreading, followed by random migration. Five to ten minutes after the onset of migration, DCs outside the coated area started to move directionally toward the chemokine spot, while *Ccr7*$^{-/-}$ DCs were unresponsive (Figures 3A–3C; Movie S3). These observations suggest that immobilized CCL21 has three effects on mature DCs: (1) it triggers rapid spreading, (2) it triggers random migration, and (3) it triggers the release of a soluble factor that attracts more DCs. We continued to dissect these individual responses in a reductionist manner.

DCs Turn Immobilized CCL21 into Soluble CCL21 that Resembles CCL19

We first addressed the nature of the soluble attractant that is produced once DCs contact CCL21. In order to physically separate the site where soluble attractant is produced from the responding cells, we performed underagarose chemotaxis assays. Here, cells and attractant are placed in distant holes of an agarose layer, which allows diffusion of solutes while the cells can migrate between agarose and substrate along soluble gradients (Heit and Kubes, 2003). In this setup, CCL21 triggered a minimal chemotactic response in mature DCs, while they migrated vigorously (and directionally) toward a mixture of CCL21 and DCs. DCs alone did not attract other DCs. This demonstrated the induction of a soluble chemotactic gradient once DCs contacted CCL21. This chemotactic response was comparable to DCs migrating toward CCL19 (Figure 4A).

Migration toward the mixture of CCL21 and DCs was blocked when the responder DCs were preincubated with pertussis toxin. Moreover, *Ccr7*$^{-/-}$ DCs were unresponsive (Figure 4A), suggesting that either an unknown CCR7 ligand, CCL19 or an altered form of CCL21 was released upon contact of CCL21 with DCs. As *plt/plt* DCs plus CCL21 and WT DCs plus CCL21 (in the absence or presence of BrefeldinA to inhibit golgi export, data not shown) triggered comparable chemotaxis (Figure 4A), the induced release of CCL19 or other proteins was excluded. We conclude that the chemotactic cue was most likely a modified variant of CCL21 itself that is produced upon direct contact between DCs and CCL21.

To test for possible modifications of CCL21, we performed immunoblot analysis of CCL21 before and after incubation with

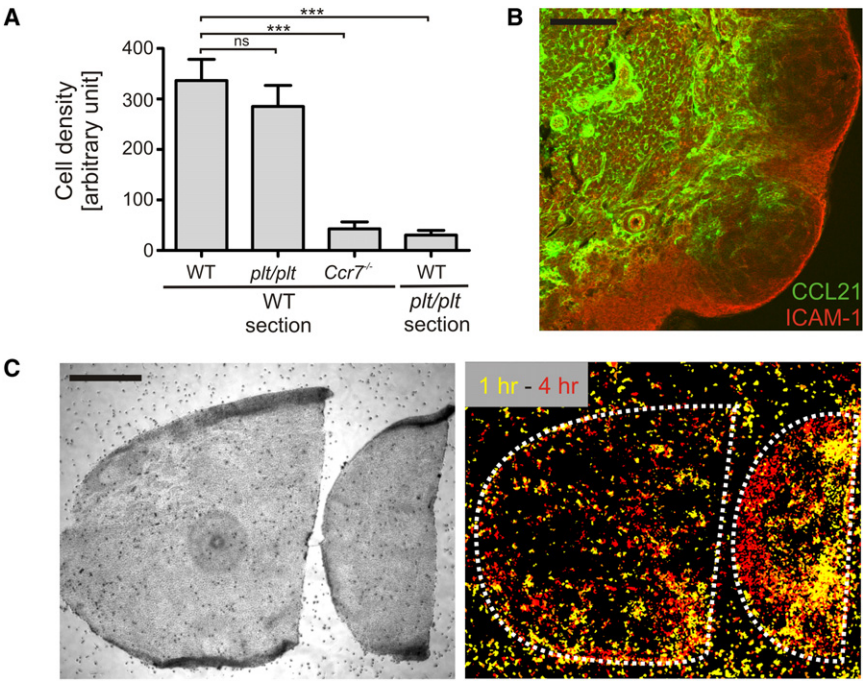

Figure 2. Dendritic Cells Are Directed by Soluble Gradients

(A) Accumulation of wild-type (WT), *Ccr7*$^{-/-}$, and *plt/plt* dendritic cells (DCs) on either WT or *plt/plt* lymph node sections. Bars represent mean ± SEM, n = 3.

(B) Fluorescent staining of a lymph node section for CCL21 (green) and ICAM-1 (red). Scale bar represents 250 μm.

(C) A peripheral part of a lymph node section was dissected, inverted by 180°, and repositioned in close proximity to the remaining part of the section. Left panel: bright-field image of the manipulated section. Right panel: Migratory course of mature DCs on this section. Different time points were colorized in graded wavelengths from yellow (1 hr) to red (4 hr) to show migrating fractions of DCs. Dotted line: outline of the section. Data represent one out of four independent experiments. Scale bar represents 200 μm. ***p < 0.001; ns, not significant.

DCs. A CCL21 fragment of approximately 8 kDa size appeared with increasing incubation times (Figure 4B), but no comparable response was seen upon incubation with naive T cells, B cells, or fibroblasts (Figure 4C). We found a comparable CCL21 fragment when we immunoprecipitated CCL21 from lymph node lysates (Figure 4D), demonstrating the potential in vivo relevance of our findings. Processing was completely blocked by the serine protease inhibitor Aprotinin (Figure 4E), but not by a wide range of other protease inhibitors (data not shown). Accordingly, the supernatant of WT DCs plus CCL21 lost its chemotactic activity in under agarose assays when Aprotinin was present (Figure 4A). To map the site of cleavage, we incubated recombinant CCL21 carrying an N-terminal Flag-tag and a C-terminal His-tag with DCs. Loss of His-tag, but not Flag-tag, immunoreactivity demonstrated cleavage of the C terminus (Figure 4F). Together, these findings demonstrate that upon direct contact with mature DCs, CCL21 is processed into a variant that lacks the heparan sulfate binding residues and is able to diffuse and act chemotactically. Cleaved CCL21 resembles native CCL19, which is neither proteolytically processed nor gains chemotactic activity upon exposure to DCs (data not shown). Accordingly, recombinant truncated CCL21 that lacked the C terminus induced strong chemotaxis (Figure 4A).

Immobilized, but Not Soluble, Chemokine Triggers Integrins on DCs

Morphology of migratory DCs on lymph node sections and on immobilized CCL21 suggested that adhesion is a critical factor for DC migration on the sections: migratory DCs were flattened and polarized, while nonmigrating DCs were rounded and dendritic (Figure 5A; Movie S4). This prompted us to test whether integrins are involved in the migration process. In contrast to negative results with all other integrin family members (data not shown), DCs generated from *Itgb2*$^{-/-}$ mice neither spread on the interfollicular areas nor accumulated in the center of sections (Figure 5B; Movie S5). We conclude that DC migration on lymph node cryosections is mediated by β2 integrin dependent adhesion. Similarly, *Ccr7*$^{-/-}$ DCs were not only unable to perform

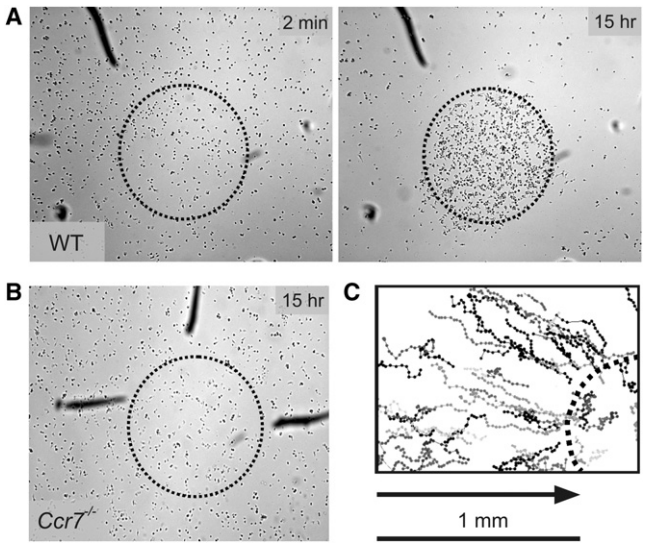

Figure 3. Migration of Dendritic Cells toward Immobilized CCL21

CCL21 was plated on cell culture plastic (coated area marked by dotted circle).

(A) Distribution of dendritic cells (DCs) on CCL21 coated area after 2 min (left panel) and 15 hr (right panel). Data show one representative out of > 30 independent experiments.

(B) *Ccr7*$^{-/-}$ DC distribution after 15 hr.

(C) Single-cell tracking of migrating WT DCs. Each track represents the pathway of a single cell over 30 min. Migration is directed toward the CCL21 coated area (arrow) and is observed in uncoated areas up to 1 mm from the coated area.

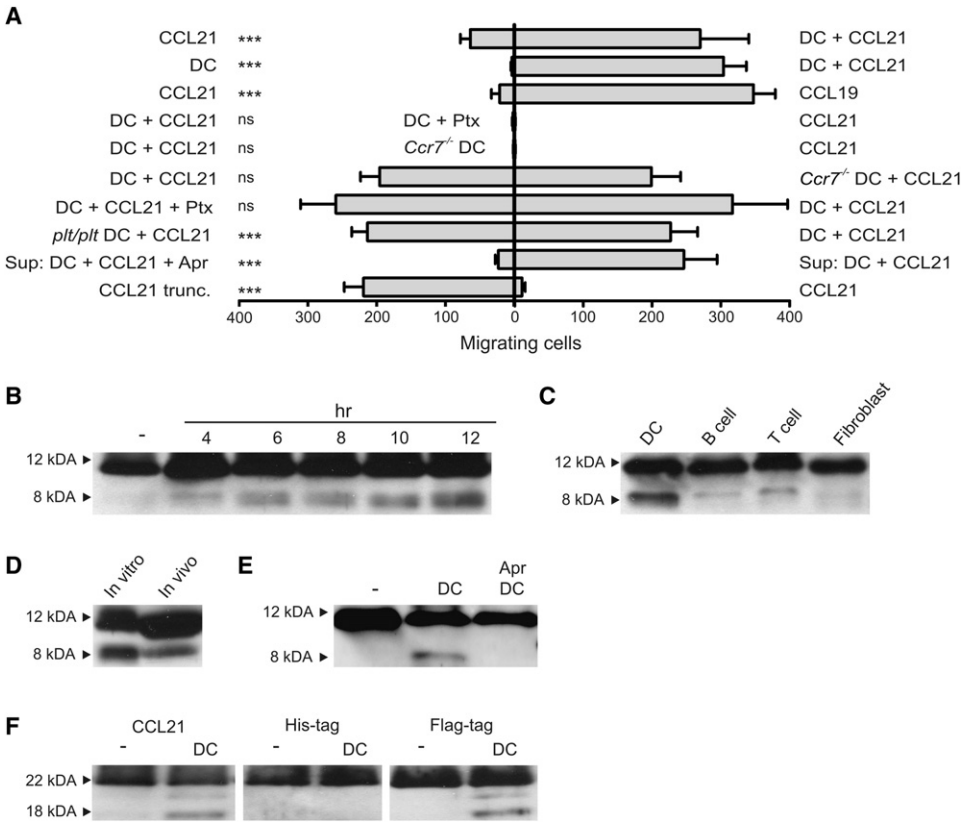

Figure 4. Dendritic Cells Turn Immobilized CCL21 into Soluble CCL21

(A) Number of migrated cells after 15 hr. Ptx, pertussis-toxin; Apr, aprotinin; Sup, cell supernatant; CCL21 trunc., CCL21 with truncated C terminus. If not otherwise indicated, WT DCs were applied. Error bars represent mean ± SEM, n = 4–8.

(B) CCL21 was incubated with DCs for up to 12 hr. Processing of CCL21 was determined by immunoblot analysis. Control (–), CCL21 incubated in medium without DCs.

(C) DCs, B cells, T cells, and fibroblasts were coincubated with CCL21 for 12 hr before immunoblot analysis of the supernatant.

(D) In vitro: CCL21 cleavage after 12 hr coincubation with DCs. In vivo: pull-down of in vivo cleaved CCL21 out of LN-lysate.

(E) CCL21 was incubated with DCs or with DCs and Aprotinin for 15 hr. Control (–): CCL21 incubated in medium without DCs.

(F) Immunoblot analysis of tagged CCL21 (detection of CCL21, His- and Flag-tag) after 15 hr incubation with DCs (+). Control (–): CCL21-incubation in medium without DCs. ***$p < 0.001$; ns, not significant.

directed migration but also remained rounded on cryosections (data not shown). This suggested that adhesiveness and chemokine sensing were functionally linked and led us to investigate the crosstalk between CCR7 and integrins on DCs. One potential β2 integrin ligand on the sections is ICAM-1, which is abundantly expressed in the T cell area (Figure 2B). WT DCs were monitored upon settling on surfaces coated with a mixture of CCL21 and ICAM-1. The cells showed rapid spreading within minutes after contact with CCL21 plus ICAM-1 (Figure 5C), while ICAM-1 alone did not trigger spreading, indicating a quiescent state of the ICAM-1 binding β2 integrins on mature DCs. When DCs were plated onto surfaces coated with both CCL19 and ICAM-1, only weak spreading was observed (Figure 5C). The same pattern emerged when both chemokines were bound to surfaces that were precoated with polysialic acid, a physiological substrate for CCL21 binding (Bax et al., 2009) (Figure S1A). Importantly, soluble CCL21 and CCL19 applied in concentrations that exceeded the amounts needed to trigger chemotactic migration did not induce any spreading response (Figure 5D). The lack of spreading on CCL19 could either be due to differential signaling properties or inefficient immobilization of CCL19 because it lacks a charged C terminus. We therefore plated the chemokines on surfaces pretreated to enhance protein-loading capacity. In this setup, where comparable amounts of CCL21 and CCL19 were immobilized (Figure S1B), CCL19 induced substantial spreading (Figure 5E). When *Itgb2*$^{-/-}$ and *Ccr7*$^{-/-}$ DCs were plated on the same cocoated surfaces, no spreading was observed (Figure 5E). These findings indicate that the interaction between CCR7 and immobilized, but not soluble, CCR7 ligand induces integrin-dependent spreading, polarization, and migration of DCs (Figure 5F).

Directional Steering of Haptokinetic Movement

The cryosection assays suggested that haptic migration on a track functionalized with CCL21 can be steered by a soluble gradient of CCR7 ligand. To directly test this in a controlled experimental setup, we established a variant of 3D collagen gel chemotaxis assays. Consistent with our above observation

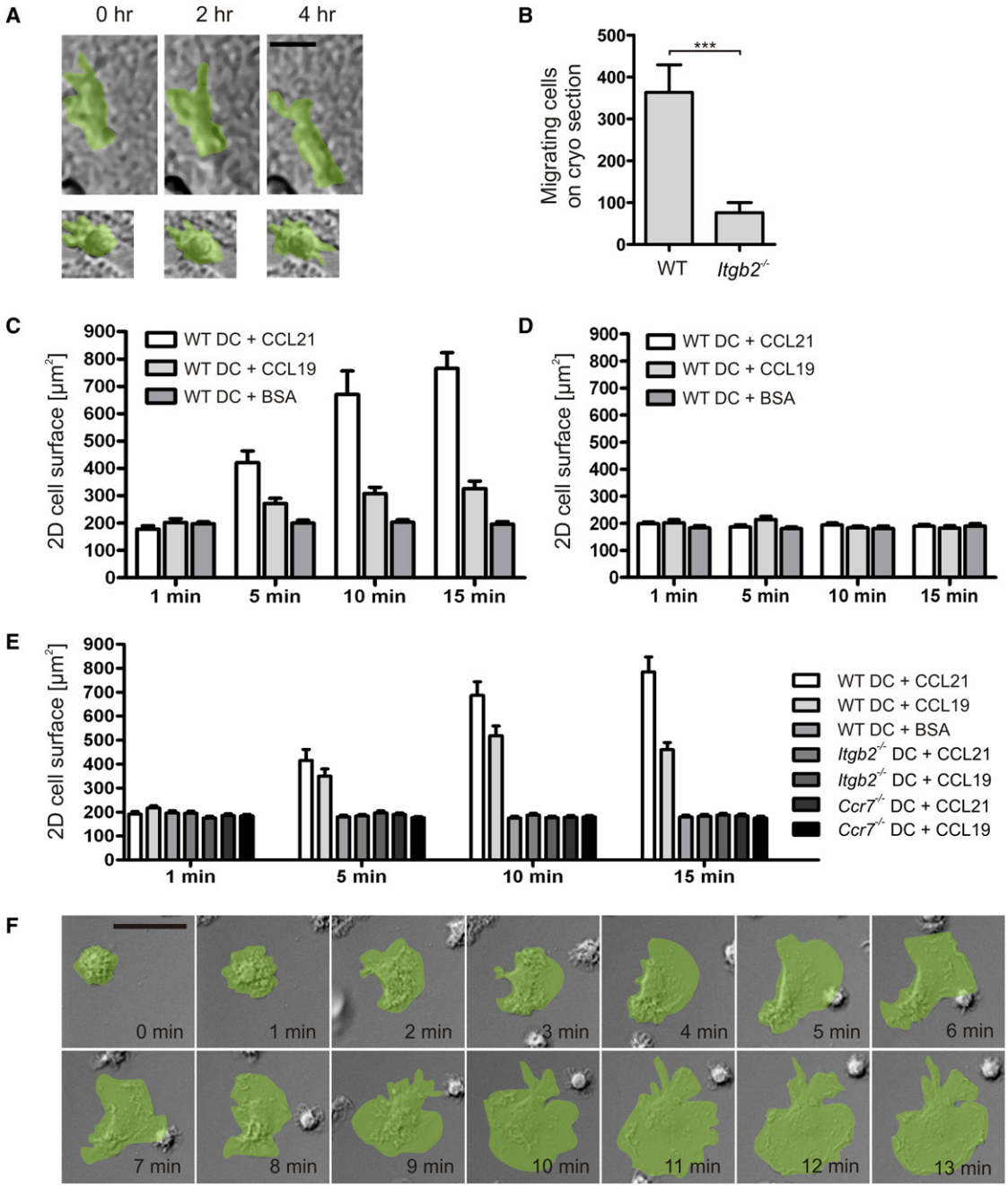

Figure 5. Immobilized chemokine causes haptokinetic migration

(A) Morphology of a dendritic cell (DC) applied to a lymph node section after 0, 2, and 4 hr. Upper panels: elongated, nondendritic "amoeboid" shape of a DC migrating on a sinus area. Lower panels: rounded, dendritic-like morphology of a nonmigrating DC on a B cell follicle. The cell surfaces are highlighted in green. Scale bar represents 10 µm.

(B) Accumulation of WT and *Itgb2*$^{-/-}$ DCs on a lymph node sections. Error bars represent mean ± SEM, n = 3.

(C) Quantification of the 2D projected cell surface after contact with either CCL21 plus ICAM-1, CCL19 plus ICAM-1, or BSA plus ICAM-1 coated glass surfaces after 1, 5, 10, and 15 min. Error bars show mean ± SEM, n = 25.

(D) 2D projected surface of DCs on ICAM-1 coated glass surfaces after 1, 5, 10, and 15 min incubation with CCL21, CCL19, or BSA applied to the medium. Error bars represent mean ± SEM, n = 25.

(E) 2D projected surface of WT, *Ccr7*$^{-/-}$, and *Itgb2*$^{-/-}$ DCs after contact with a plasma-treated and subsequently CCL21 plus ICAM-1, CCL19 plus ICAM-1, or BSA plus ICAM-1 coated glass surface after 1, 5, 10, and 15 min. Error bars represent mean ± SEM, n = 25.

(F) Outline of a DC polarizing on a CCL21 plus ICAM-1-spot over 13 min. The surface of the DC is highlighted in green. Scale bar represents 25 µm. ***$p < 0.001$.

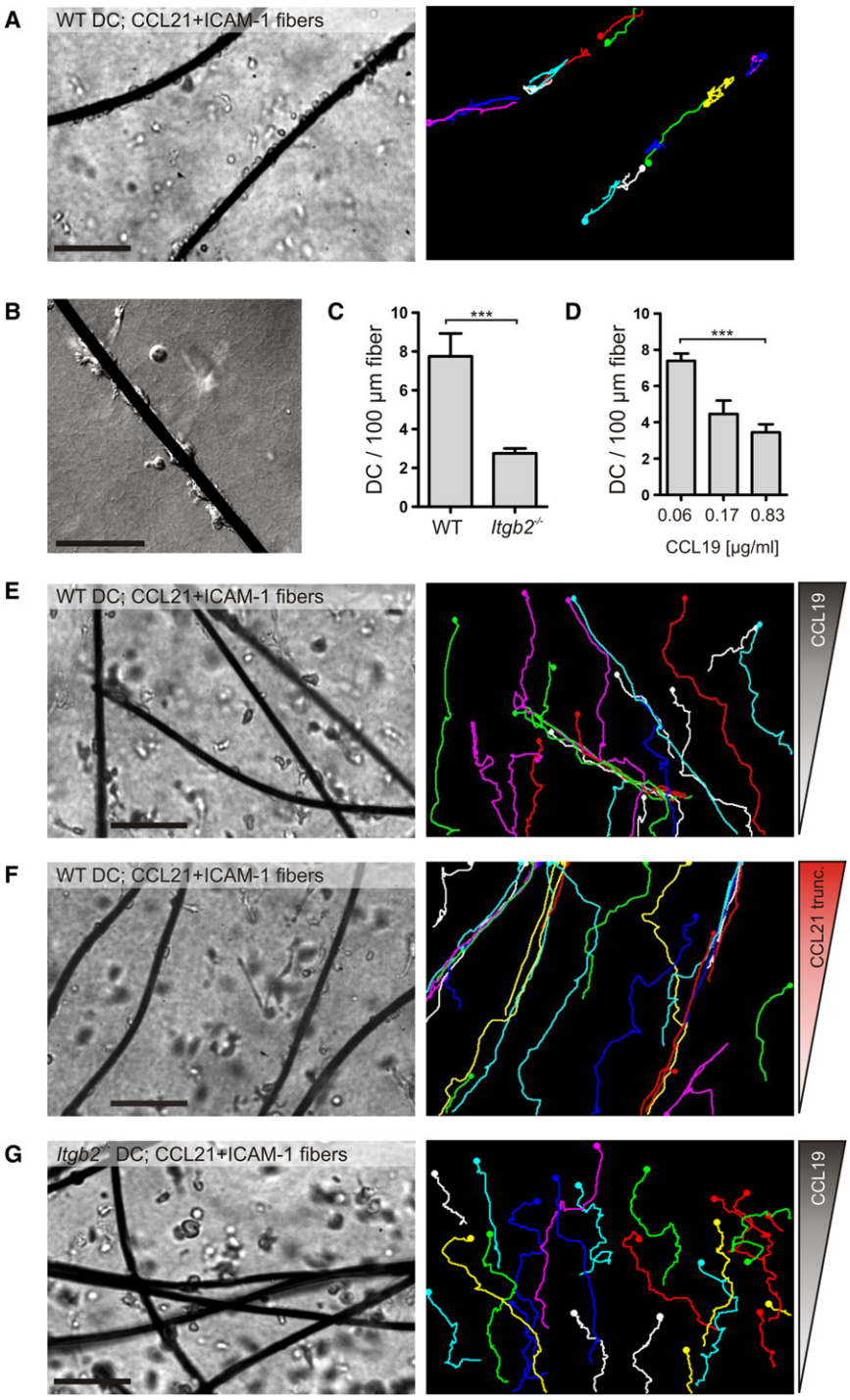

Figure 6. Soluble Chemokine Steers Haptokinetic Migration

Three-dimensional collagen gel assays with incorporated protein-coated carbon microfibers. (A, E, F, and G) Left panels: bright-field image of the collagen gel with coated fibers. Right panels: single-cell tracking of dendritic cells (DCs). Here, each colored track represents the pathway of a single cell.

(A) DCs in the presence of CCL21/ICAM-1-coated carbon fibers.

(B) Differential interference contrast image of DCs spreading on a CCL21 plus ICAM-1-coated fiber. Scale bar represents 50 μm.

(C) Quantification of WT and *Itgb2*$^{-/-}$ DCs associated with CCL21 plus ICAM-1-coated fibers after 5 hr incubation. Bars represent mean ± SEM, n = 5.

(D) Quantification of WT DCs associated with with CCL21 plus ICAM-1 coated fibers after 5 hr incubation in a collagen gel with different CCL19 gradients applied. Bars represent mean ± SEM, n = 4.

(E) Directionally biased DCs migration on CCL21 plus ICAM-1 coated fibers within a CCL19 gradient. DCs remote from coated fibers migrate through the collagen gel toward the CCL19 gradient.

(F) WT DCs migrating with a directional bias in a collagen gel with CCL21 plus ICAM-1-coated fibers toward a gradient of truncated CCL21.

(G) *Itgb2*$^{-/-}$ DCs migrating in a collagen gel with CCL21 plus ICAM-1-coated fibers and applied CCL19-gradient. ***p < 0.001.

that soluble chemokine does not activate integrins, DCs migrate in a nonadhesive and integrin-independent manner when they are exposed to soluble gradients of CCL19 within the gels (Lämmermann et al., 2008). To mimic chemokinetic interfaces, we incorporated carbon microfibers (5 μm diameter) that were previously cocoated with ICAM-1 and CCL21 into the gels. Once in contact with the fibers, DCs adhered to the surface and moved up and down frequently switching directionality, while uncoated fibers were ignored (Figures 6A and 6B; Movies S6 and S7). *Itgb2*$^{-/-}$ DCs did not associate with the coated fibers (Figure 6C). To test if the haptokinetic cells on the fibers were still responsive to directional stimuli, we introduced soluble gradients of either CCL19 or truncated CCL21 into the gel. As shown previously, this caused directionally persistent chemotactic migration of the non-fiber-associated DCs. Importantly, the soluble gradient directionally biased the DCs on the fibers: once cells contacted a fiber, they preferred to follow its surface even if they were distracted from the direct path (Figures 6E and 6F and Movies S8 and S9). With increasing concentrations of soluble CCL19, less DCs remained on the fibers, suggesting that chemotactic and adhesive signals compete (Figure 6D). Fibers coated with ICAM-1 alone were ignored by the DCs, confirming our previous results that soluble CCR7 ligand does not trigger adhesion. Accordingly, when *Itgb2*$^{-/-}$ DCs were employed in the assays, they showed no interaction with CCL21 plus ICAM-1 cofunctionalized fibers but moved with normal speed and directionality within the gels (Figure 6G; Movie S10), as expected from our previous studies (Lämmermann et al., 2008).

These results demonstrate that DCs respond to immobilized CCL21 fields haptokinetically while simultaneously sensing a soluble gradient of CCR7 ligand that introduces a directional bias.

DISCUSSION

We have shown that in mature DCs, surface-immobilized CCL21 induces both inside-out activation of β2 integrins and cytoskeletal polarization, which results in haptokinetic movement. CCL19, which does not immobilize to surfaces because it lacks a heparan sulfate binding C terminus, does not induce adhesion but does polarize the cytoskeleton and therefore causes chemotactic movement. When both immobilized and soluble chemokines were offered, DCs showed a combined response and performed directionally biased haptokinetic migration. By proteolytically truncating the heparan sulfate binding residue and thereby generating a soluble form of CCL21, DCs generated a self-perpetuating wave of collective migration where immobilized CCL21 dictated the pathway and either solubilized CCL21 or CCL19 the direction of migration.

We demonstrated this principle using reductionist in vitro setups. However, the combination of haptokinesis and chemotaxis potentially explains many phenomena that have been observed in vivo, and the principle might apply to lymphocytes as well as DCs. Using intravital or tissue-slice microscopy, it was shown that both blocking of Gαi protein-coupled chemokine receptors or the deletion of CCR7 impaired the movement of naive T cells and mature DCs in the lymph node (Asperti-Boursin et al., 2007; Okada and Cyster, 2007; Worbs et al., 2007). Hence, chemokine signals are essential for both triggering and maintaining an optimal motile state. Recent intravital microscopy studies provided an extension to this view and demonstrated that the three-dimensional scaffolds of T cell area FRCs and the B cell area follicular dendritic cells represent the tracks along which T and B cells migrate, respectively (Bajénoff et al., 2006, 2007, 2008; Roozendaal et al., 2009). Interestingly, migration on the tracks lacked any directional bias, resulting in "guided randomness" (Mempel et al., 2006), a swarming locomotion pattern within strictly segregated compartments. Mechanistically, it was suggested that CCL21 that is produced by and immobilized on the FRC surface might form a field that keeps the cells motile (Bajénoff et al., 2006). The same was suggested for CXCL13 on B cell follicle stroma cells (Roozendaal et al., 2009). However, a kinetic stroma-scaffold alone does not sufficiently explain such behavior. The scaffold additionally has to be adhesive, otherwise the cells would lose surface contact and would "fall off the tracks." The haptokinetic migration mode we describe here perfectly explains the above in vivo findings.

The haptokinetic scaffold is conceptually appealing as an immobilized and therefore static chemokine field and is potentially robust against the convective forces, turbulences, and mechanical perturbations in vivo. While this principle explains homeostatic swarming, it also has limitations: it lacks any directional information and does not allow for local regulation. Most importantly, it does not explain the following phenomena that have been described in vivo: (1) After penetrating the floor of the subcapsular sinus, DCs migrate directionally around the B cell follicles into the deeper T cell regions (Lämmermann et al., 2008; Sumen et al., 2004). (2) Upon activation, B cells upregulate CCR7 and move directionally toward the interface between T and B area, and the experimental introduction of CCR7 into naive B cells has the same effect (Okada et al., 2005; Reif et al., 2002). (3) Upon lymph node entry, epidermis-derived DCs that only express CCR7 settle in the deep T cell area (Kissenpfennig et al., 2005; Saeki et al., 2000; Wu and Hwang, 2002), while dermis-derived DCs that express both CCR7 and CXCR5 (Saeki et al., 2000) move to areas closer to the B cell follicles. These and other in vivo reports of directional migration within lymphatic organs (Castellino et al., 2006; Chtanova et al., 2008; Okada et al., 2005), together with in vitro findings that T cells, B cells, and DCs are all capable to migrate toward spatial chemokine gradients (Worbs et al., 2007; Lämmermann et al., 2008, 2009), strongly argue for the presence of graded distributions of chemokines within lymphatic organs that serve not only as motility triggers but also as long-range directional cues.

The directionally biased haptokinesis that we describe here resolves the dilemma between the kinetic and the tactic model as it combines the robustness of haptokinesis with the flexibility of chemotaxis. It also harbors many regulatory possibilities that we did not directly address in our reductionist approach. Physiological phenomena such as blurred borders between T and B cell area during inflammatory responses (Okada et al., 2005) might well be caused by shifting the balance between soluble and bound CCR7 ligand as in the example caused by the proteolytic shedding of CCL21 that we describe. In this context it is interesting that the chemotactic "pull" of a soluble gradient counteracts adhesion to the immobilized chemokine and vice-versa. This means that either steep soluble gradients or sparse CCL21 and integrin-ligand coating of the FRCs might, depending on the chemokine receptor expression level of the responding cell, individually influence intranodal positioning and also dwell times of cell populations within the lymph node. It was shown that stroma cells of reactive lymph nodes downregulate the transcription of homeostatic chemokines, leading to reduced T cell priming during secondary immunizations (Mueller et al., 2007). Shedding of CCL21 might act similarly, even before such transcriptional responses occur, and possibly causes local micromilieus within the reactive lymph node. Solubilization of chemokines might further support collective movement patterns as they have been described for DCs: here, migrating cells locally recruit more cells into the lymph node, a phenomenon that has been described as lymph node conditioning (Martín-Fontecha et al., 2003).

From a cell biological perspective, kinesis is the product of either spontaneous or externally triggered self-polarization. Self-polarization does not rely on asymmetrical external cues and thereby causes cytoskeletal rearrangements and migration in a random direction (Andrew and Insall, 2007; Wedlich-Soldner and Li, 2003). Recently, it has been proposed that self-polarization and directed migration might be more closely connected than previously considered. Arrieumerlou et al. proposed a model that describes directed movement as a phenomenon that is superimposed on self-polarization. Here, every chemokine-triggered signaling event that occurs within one of many leading edge protrusions of a self-polarized cell leads to local re-enforcement of the protrusion. Consequently, an initially random migrating cell gradually turns toward the source of

the chemotactic cue and thereby performs a "directionally biased random walk" that shows increasing directional persistence with increasing steepness of the gradient (Arrieumerlou and Meyer, 2005). The directionally steered haptokinesis we observed in the present study can be viewed as an extension of this model, where immobilized CCL21 triggers adhesion as well as random polarization and migration, while soluble chemokine gradients introduce a directional bias (see schematic in Figure S2).

Apart from offering a cell biological explanation for observed phenomena of intranodal leukocyte migration, our findings might be of more general relevance. We have recently shown that leukocytes are able to migrate with identical velocities in the adhesive and nonadhesive mode because they efficiently adapt their cytoskeletal dynamics (Renkawitz et al., 2009). Although this means that integrins are not essential for actual movement, they can shape the migratory pathway and also mediate close contact with surfaces while the cell moves. This makes physiological sense because diffusive distribution of soluble cues is largely unaffected by extracellular matrix components. Cells that are nonadherent can directly follow these cues without being "distracted" by the local cellular or extracellular infrastructure. Only once it is decorated with an immobilized chemokine that activates integrin-mediated anchoring, the infrastructure becomes adhesive and therefore affects the behavior of the cell.

EXPERIMENTAL PROCEDURES

Reagents

Chemokines: recombinant murine CCL19 and CCL21 and murine ICAM-1 humanFc fusion protein were purchased from R&D Systems. For immunofluorescence polyclonal rabbit anti-mouse laminin 111 (Sixt et al., 2005), rabbit anti-mouse Exodus-2 (PeproTech) monoclonal hamster anti ICAM-1 (PharMingen) were used. Primary antibodies were detected using FITC- or Cy3-conjugated goat anti-rat or goat anti-rabbit IgG (Dianova). Primary antibodies employed for immunoblot analysis were as follows: rabbit anti-mouse Exodus-2 (PeproTech), mouse anti-His-Tag (Novagen), and anti-Flag M2-Peroxidase (Sigma-Aldrich). Anti-rabbit horseradish peroxidase (HRP) and anti-mouse-HRP (both Biorad) were used as secondaries.

Mice

Itgb2$^{-/-}$ (Wilson et al., 1993), *Ccr7*$^{-/-}$ (Förster et al., 1999), and *plt/plt* mice (Nakano et al., 1998) were kept on a C57BL/6 background and bred in a conventional animal facility according to the local regulations.

Generation of Bone Marrow-Derived DC

DCs were generated from flushed bone marrow as described previously (Lutz et al., 1999). Maturation was induced overnight with 200 ng/ml LPS (Sigma-Aldrich; *E. coli*; 0127:B8) on days 9–11 of culture. All experiments with DCs were performed in R10 medium (RPMI supplemented with 10% fetal calf serum [FCS] [both Invitrogen; FCS heat-inactivated for 20 min at 57°C], penicillin-streptomycin, and glutamine [PAA]).

Immunofluorescence Microscopy

Cryostat sections (8 μm) were fixed in methanol at −20° for 10 min, blocked with 1% BSA, and subjected to standard immunofluorescence staining procedures. Stained sections were examined using either a Zeiss Axiophot fluorescence microscope and documented with the Openlab software version 3.1.2 (Improvision) or an inverted confocal microscope (Leica, SP2).

In Vivo Migration of DCs

Mature DCs were labeled with 5 μM 5-, 6-carboxyfluorescein diacetate succiniminidyl ester (CFSE) according to the manufacturer's recommendations (Molecular Probes). After labeling and extensive washing in phosphate buffered saline (PBS), 5 × 10^5 DCs in a volume of 20 μl PBS were injected into the hind footpads. Draining lymph nodes were harvested and snap-frozen in liquid nitrogen.

Production of Recombinant Chemokines

Tagged recombinant CCL21 was produced using the *Pichia pastoris* yeast expression system (Invitrogen). The coding sequence of mature CCL21 (amino acids 24–133) was PCR-amplified from pET52-CCL21 (forward: 5′-ACG TAG AAT TCC GAC TAC AAG GAC GAC GAT GAC AAG AGT GAT GGA GGG GGT CAG GAC-3′; reverse: 5′-TAC GTA TCT AGA GG TCC TCT TGA GGG CTG TGT CTG-3′). The product was cloned into pPICZαC (Invitrogen), and the plasmid linearized with ScaI (NEB) and transfected into *P. pastoris SMD1168H* (Invitrogen). CCL21 was purified from the yeast culture supernatant using NTA agarose (RAQ007.2, QIAGEN).

Full-length and C-terminally truncated CCL21 (amino acids 24–98) were PCR-amplified introducing a stop codon (forward: full-length and truncated mCCL21: 5′-CAAGGTCTCAGGTGGTAGTGATGGAGGGGGTCAG; reverse: full-length, 5′- CAGCTCGAGTCATCCTCTTGAGGGCTGTGTCTG; truncated, 5′-AATCTCGAGTCATTTCCCTGGGGCTGGAGG). PCR fragments were cloned into pET-6his-SUMO-1. Transformed *E. coli* B834(DE3)pLysS (Novagen) were disrupted (Constant Systems Ltd.), supernatants were loaded on a HisTrap HP column (GE Healthcare), and bound proteins were eluted with PBS containing 500 mM imidazole using an AKTA Explorer chromatography system (Amersham Biosciences). Eluted fractions were digested with a C-terminal his-tagged Ubl-specific protease 1 (ULP1) at 4°C followed by purification of cleaved chemokines in a Zn^{2+} charged HiTrap IMAC FF column (GE Healthcare) and optional gel filtration (HiPrep Sephacryl S-200, GE Healthcare).

Analysis of Chemokine Cleavage

150 ng of untagged CCL21 (R&D Systems) or 75 ng tagged CCL21 (expressed in *P. pastoris*) were incubated with 6 × 10^5 DCs in 100 μl R10-medium for 4–12 hr at 37°C, 5% CO_2. The proteins in the cell supernatants were separated by SDS-PAGE on 15% Tris-lysine-gels and blotted on PVDF membrane (Immobilon, 0.2 μm, Millipore). Membranes were blocked with PBS containing 5% BSA (PAA), and consecutively incubated with first antibody and HRP-conjugated secondary antibody. Signal was detected using Western Lightning Chemiluminescence Reagent Plus (PerkinElmer). For CCL21 pull-down from lymph node-lysate popliteal, inguinal and axillary LNs were harvested and sonicated in lysis buffer (50 mM Tris [pH 8], 150 mM NaCl, 10 mM EDTA, 0.05% Desoxycholate, 1% Triton, and protease inhibitor cocktail [Roche]). For antibody binding, ProteinG Dynabeads were incubated in washing buffer (PBS [pH 7.4] with 1% Triton) containing rabbit anti-mouse Exodus-2 (PeproTech). After extensive washing, beads were incubated with the lysate and subsequently washed and resuspended in 6× SDS-PAGE sample buffer, heated at 95°C for 10 min, and analyzed by SDS-PAGE.

In Vitro Migration Assays

For migration on cryosections mouse inguinal lymph nodes were snap-frozen in liquid nitrogen. Eight to ten μm thick sections were collected on glass slides. The slides with the section were then immobilized on the bottom of a custom-built migration chamber, covered with DCs in R10 medium, and observed by time-lapse video microscopy. For migration on chemokine spots, custom-made glass bottom cell culture dishes were either left untreated or incubated for 1 min in a plasma cleaner. A drop containing 22.5 μg/ml CCL21 or CCL19 and 10 μg/ml ICAM-1 was incubated on a coverslip (optionally precoated with 10 μg/ml polySia [Sigma-Aldrich]) in PBS for 30 min at 37°C. After washing with PBS, the surface was covered with 1 × 10^6 DCs/ml in a custom built incubation chamber. The surface area of the cells was documented after 1, 5, 10, and 15 min. Underagarose assays were performed as described previously (Heit and Kubes, 2003). Wells (volume approx. 7 μl) were filled with 6 × 10^4 DCs and/or 625 ng/ml CCL19, CCL21, or truncated CCL21. Pertussis-Toxin (List Biochemicals) was applied at 20 μg/ml, and Aprotinin (Calbiochem) was applied at 150 μM. After 15 hr at 37°C, 5% CO_2, cells that migrated out of the "responder" hole were photographed using a Zeiss Axiovert 40 CFL microscope and manually counted. Collagen assays were performed as described previously (Lämmermann et al., 2008) with a collagen concentration of 1.6 mg/ml and 10^6 DCs/ml. The gels were cast in a custom-made chamber

(thickness of 2 mm) with protein-coated carbon fibers (BP 2308, BALTIC). For coating, fibers were incubated with 5 μg/ml ICAM-1 and either 0.1% BSA (PAA),5 μg/ml CCL21 or CCL19. Polymerized gels were covered with R10-medium or R10-medium containing 0.17 μg/ml CCL19 or 0.54 μg/ml truncated CCL21 and observed by time-lapse video microscopy.

Image Processing

Color-coded composites were generated by superimposing background-subtracted binary layers using Openlab software version 3.1.2 (Improvision). Automated cell counting was done by creating background-subtracted binary layers and subsequent automated pixel density measurements in the marked areas using Openlab software. Single-cell tracking and surface measurements of cells were either done with the classification module of Volocity software version 2.5 (Improvision) or ImageJ software employing the "Manual Tracking Plugin" (http://rsbweb.nih.gov/ij/). Surface measurements were done with Metamorph software (Molecular Devices).

Statistical Analysis

Student's t tests and analysis of variance (ANOVA) were performed after data were confirmed to fulfill the criteria of normal distribution and equal variance. Analyses were performed with Sigma Stat 2.03.

SUPPLEMENTAL INFORMATION

The Supplemental Information includes two figures and ten movies and can be found with this article online at doi:10.1016/j.immuni.2010.04.017.

ACKNOWLEDGMENTS

This work was funded by the Peter Hans Hofschneider Foundation for Experimental Biomedicine, the German Research Foundation, the Max Planck Society, the Swiss National Science Foundation, the Max Cloëtta Foundation, the ELAN Fond of the University of Erlangen, and European Union Marie Curie Fellowships to M.S. and J.P. We thank the members of the Sixt laboratory for discussions and critical reading of the manuscript, N. Catone for technical assistance, and R. Fässler for continuous support.

Received: July 14, 2009
Revised: February 10, 2010
Accepted: April 30, 2010
Published online: May 13, 2010

REFERENCES

Alvarez, D., Vollmann, E.H., and von Andrian, U.H. (2008). Mechanisms and consequences of dendritic cell migration. Immunity *29*, 325–342.

Andrew, N., and Insall, R.H. (2007). Chemotaxis in shallow gradients is mediated independently of PtdIns 3-kinase by biased choices between random protrusions. Nat. Cell Biol. *9*, 193–200.

Arrieumerlou, C., and Meyer, T. (2005). A local coupling model and compass parameter for eukaryotic chemotaxis. Dev. Cell *8*, 215–227.

Asperti-Boursin, F., Real, E., Bismuth, G., Trautmann, A., and Donnadieu, E. (2007). CCR7 ligands control basal T cell motility within lymph node slices in a phosphoinositide 3-kinase-independent manner. J. Exp. Med. *204*, 1167–1179.

Bajénoff, M., Egen, J.G., Koo, L.Y., Laugier, J.P., Brau, F., Glaichenhaus, N., and Germain, R.N. (2006). Stromal cell networks regulate lymphocyte entry, migration, and territoriality in lymph nodes. Immunity *25*, 989–1001.

Bajénoff, M., Egen, J.G., Qi, H., Huang, A.Y., Castellino, F., and Germain, R.N. (2007). Highways, byways and breadcrumbs: directing lymphocyte traffic in the lymph node. Trends Immunol. *28*, 346–352.

Bajénoff, M., Glaichenhaus, N., and Germain, R.N. (2008). Fibroblastic reticular cells guide T lymphocyte entry into and migration within the splenic T cell zone. J. Immunol. *181*, 3947–3954.

Bax, M., van Vliet, S.J., Litjens, M., García-Vallejo, J.J., and van Kooyk, Y. (2009). Interaction of polysialic acid with CCL21 regulates the migratory capacity of human dendritic cells. PLoS ONE *9*, e6987. 10.1371/journal.pone.0006987.

Castellino, F., Huang, A.Y., Altan-Bonnet, G., Stoll, S., Scheinecker, C., and Germain, R.N. (2006). Chemokines enhance immunity by guiding naive CD8+ T cells to sites of CD4+ T cell-dendritic cell interaction. Nature *440*, 890–895.

Chtanova, T., Schaeffer, M., Han, S.J., van Dooren, G.G., Nollmann, M., Herzmark, P., Chan, S.W., Satija, H., Camfield, K., Aaron, H., et al. (2008). Dynamics of neutrophil migration in lymph nodes during infection. Immunity *29*, 487–496.

de Paz, J.L., Moseman, E.A., Noti, C., Polito, L., von Andrian, U.H., and Seeberger, P.H. (2007). Profiling heparin-chemokine interactions using synthetic tools. ACS Chem. Biol. *2*, 735–744.

Förster, R., Schubel, A., Breitfeld, D., Kremmer, E., Renner-Müller, I., Wolf, E., and Lipp, M. (1999). CCR7 coordinates the primary immune response by establishing functional microenvironments in secondary lymphoid organs. Cell *99*, 23–33.

Friedl, P., Entschladen, F., Conrad, C., Niggemann, B., and Zänker, K.S. (1998). CD4+ T lymphocytes migrating in three-dimensional collagen lattices lack focal adhesions and utilize beta1 integrin-independent strategies for polarization, interaction with collagen fibers and locomotion. Eur. J. Immunol. *28*, 2331–2343.

Friedl, P., Borgmann, S., and Bröcker, E.B. (2001). Amoeboid leukocyte crawling through extracellular matrix: lessons from the Dictyostelium paradigm of cell movement. J. Leukoc. Biol. *70*, 491–509.

Heit, B., and Kubes, P. (2003). Measuring chemotaxis and chemokinesis: the under-agarose cell migration assay. Sci. STKE *2003*, PL5.

Hirose, J., Kawashima, H., Swope Willis, M., Springer, T.A., Hasegawa, H., Yoshie, O., and Miyasaka, M. (2002). Chondroitin sulfate B exerts its inhibitory effect on secondary lymphoid tissue chemokine (SLC) by binding to the C-terminus of SLC. Biochim. Biophys. Acta *1571*, 219–224.

Junt, T., Scandella, E., Förster, R., Krebs, P., Krautwald, S., Lipp, M., Hengartner, H., and Ludewig, B. (2004). Impact of CCR7 on priming and distribution of antiviral effector and memory CTL. J. Immunol. *173*, 6684–6693.

Kissenpfennig, A., Henri, S., Dubois, B., Laplace-Builhé, C., Perrin, P., Romani, N., Tripp, C.H., Douillard, P., Leserman, L., Kaiserlian, D., et al. (2005). Dynamics and function of Langerhans cells in vivo: dermal dendritic cells colonize lymph node areas distinct from slower migrating Langerhans cells. Immunity *22*, 643–654.

Kohout, T.A., Nicholas, S.L., Perry, S.J., Reinhart, G., Junger, S., and Struthers, R.S. (2004). Differential desensitization, receptor phosphorylation, beta-arrestin recruitment, and ERK1/2 activation by the two endogenous ligands for the CC chemokine receptor 7. J. Biol. Chem. *279*, 23214–23222.

Lämmermann, T., Bader, B.L., Monkley, S.J., Worbs, T., Wedlich-Söldner, R., Hirsch, K., Keller, M., Förster, R., Critchley, D.R., Fässler, R., and Sixt, M. (2008). Rapid leukocyte migration by integrin-independent flowing and squeezing. Nature *453*, 51–55.

Lämmermann, T., Renkawitz, J., Wu, X., Hirsch, K., Brakebusch, C., and Sixt, M. (2009). Cdc42-dependent leading edge coordination is essential for interstitial dendritic cell migration. Blood *113*, 5703–5710.

Ley, K., Laudanna, C., Cybulsky, M.I., and Nourshargh, S. (2007). Getting to the site of inflammation: the leukocyte adhesion cascade updated. Nat. Rev. Immunol. *7*, 678–689.

Luther, S.A., Tang, H.L., Hyman, P.L., Farr, A.G., and Cyster, J.G. (2000). Coexpression of the chemokines ELC and SLC by T zone stromal cells and deletion of the ELC gene in the plt/plt mouse. Proc. Natl. Acad. Sci. USA *97*, 12694–12699.

Luther, S.A., Bidgol, A., Hargreaves, D.C., Schmidt, A., Xu, Y., Paniyadi, J., Matloubian, M., and Cyster, J.G. (2002). Differing activities of homeostatic chemokines CCL19, CCL21, and CXCL12 in lymphocyte and dendritic cell recruitment and lymphoid neogenesis. J. Immunol. *169*, 424–433.

Lutz, M.B., Kukutsch, N., Ogilvie, A.L., Rössner, S., Koch, F., Romani, N., and Schuler, G. (1999). An advanced culture method for generating large quantities

of highly pure dendritic cells from mouse bone marrow. J. Immunol. Methods *223*, 77–92.

Martín-Fontecha, A., Sebastiani, S., Höpken, U.E., Uguccioni, M., Lipp, M., Lanzavecchia, A., and Sallusto, F. (2003). Regulation of dendritic cell migration to the draining lymph node: impact on T lymphocyte traffic and priming. J. Exp. Med. *198*, 615–621.

Mellman, I., and Steinman, R.M. (2001). Dendritic cells: specialized and regulated antigen processing machines. Cell *106*, 255–258.

Mempel, T.R., Junt, T., and von Andrian, U.H. (2006). Rulers over randomness: stroma cells guide lymphocyte migration in lymph nodes. Immunity *25*, 867–869.

Middleton, J., Neil, S., Wintle, J., Clark-Lewis, I., Moore, H., Lam, C., Auer, M., Hub, E., and Rot, A. (1997). Transcytosis and surface presentation of IL-8 by venular endothelial cells. Cell *91*, 385–395.

Miyasaka, M., and Tanaka, T. (2004). Lymphocyte trafficking across high endothelial venules: dogmas and enigmas. Nat. Rev. Immunol. *4*, 360–370.

Mueller, S.N., Hosiawa-Meagher, K.A., Konieczny, B.T., Sullivan, B.M., Bachmann, M.F., Locksley, R.M., Ahmed, R., and Matloubian, M. (2007). Regulation of homeostatic chemokine expression and cell trafficking during immune responses. Science *317*, 670–674.

Nakano, H., Mori, S., Yonekawa, H., Nariuchi, H., Matsuzawa, A., and Kakiuchi, T. (1998). A novel mutant gene involved in T-lymphocyte-specific homing into peripheral lymphoid organs on mouse chromosome 4. Blood *91*, 2886–2895.

Ohl, L., Mohaupt, M., Czeloth, N., Hintzen, G., Kiafard, Z., Zwirner, J., Blankenstein, T., Henning, G., and Förster, R. (2004). CCR7 governs skin dendritic cell migration under inflammatory and steady-state conditions. Immunity *21*, 279–288.

Okada, T., and Cyster, J.G. (2007). CC chemokine receptor 7 contributes to Gi-dependent T cell motility in the lymph node. J. Immunol. *178*, 2973–2978.

Okada, T., Miller, M.J., Parker, I., Krummel, M.F., Neighbors, M., Hartley, S.B., O'Garra, A., Cahalan, M.D., and Cyster, J.G. (2005). Antigen-engaged B cells undergo chemotaxis toward the T zone and form motile conjugates with helper T cells. PLoS Biol. *3*, e150. 10.1371/journal.pbio.0030150.

Patel, D.D., Koopmann, W., Imai, T., Whichard, L.P., Yoshie, O., and Krangel, M.S. (2001). Chemokines have diverse abilities to form solid phase gradients. Clin. Immunol. *99*, 43–52.

Pruenster, M., Mudde, L., Bombosi, P., Dimitrova, S., Zsak, M., Middleton, J., Richmond, A., Graham, G.J., Segerer, S., Nibbs, R.J., and Rot, A. (2009). The Duffy antigen receptor for chemokines transports chemokines and supports their promigratory activity. Nat. Immunol. *10*, 101–108.

Reif, K., Ekland, E.H., Ohl, L., Nakano, H., Lipp, M., Förster, R., and Cyster, J.G. (2002). Balanced responsiveness to chemoattractants from adjacent zones determines B-cell position. Nature *416*, 94–99.

Renkawitz, J., Schumann, K., Weber, M., Lämmermann, T., Pflicke, H., Piel, M., Polleux, J., Spatz, J.P., and Sixt, M. (2009). Adaptive force transmission in amoeboid cell migration. Nat. Cell Biol. *11*, 1438–1443.

Roozendaal, R., Mempel, T.R., Pitcher, L.A., Gonzalez, S.F., Verschoor, A., Mebius, R.E., von Andrian, U.H., and Carroll, M.C. (2009). Conduits mediate transport of low-molecular-weight antigen to lymph node follicles. Immunity *30*, 264–276.

Rot, A., and von Andrian, U.H. (2004). Chemokines in innate and adaptive host defense: basic chemokinese grammar for immune cells. Annu. Rev. Immunol. *22*, 891–928.

Saeki, H., Wu, M.T., Olasz, E., and Hwang, S.T. (2000). A migratory population of skin-derived dendritic cells expresses CXCR5, responds to B lymphocyte chemoattractant in vitro, and co-localizes to B cell zones in lymph nodes in vivo. Eur. J. Immunol. *30*, 2808–2814.

Sallusto, F., Schaerli, P., Loetscher, P., Schaniel, C., Lenig, D., Mackay, C.R., Qin, S., and Lanzavecchia, A. (1998). Rapid and coordinated switch in chemokine receptor expression during dendritic cell maturation. Eur. J. Immunol. *28*, 2760–2769.

Shamri, R., Grabovsky, V., Gauguet, J.M., Feigelson, S., Manevich, E., Kolanus, W., Robinson, M.K., Staunton, D.E., von Andrian, U.H., and Alon, R. (2005). Lymphocyte arrest requires instantaneous induction of an extended LFA-1 conformation mediated by endothelium-bound chemokines. Nat. Immunol. *6*, 497–506.

Sixt, M., Kanazawa, N., Selg, M., Samson, T., Roos, G., Reinhardt, D.P., Pabst, R., Lutz, M.B., and Sorokin, L. (2005). The conduit system transports soluble antigens from the afferent lymph to resident dendritic cells in the T cell area of the lymph node. Immunity *22*, 19–29.

Stein, J.V., Rot, A., Luo, Y., Narasimhaswamy, M., Nakano, H., Gunn, M.D., Matsuzawa, A., Quackenbush, E.J., Dorf, M.E., and von Andrian, U.H. (2000). The CC chemokine thymus-derived chemotactic agent 4 (TCA-4, secondary lymphoid tissue chemokine, 6Ckine, exodus-2) triggers lymphocyte function-associated antigen 1-mediated arrest of rolling T lymphocytes in peripheral lymph node high endothelial venules. J. Exp. Med. *191*, 61–76.

Sumen, C., Mempel, T.R., Mazo, I.B., and von Andrian, U.H. (2004). Intravital microscopy: visualizing immunity in context. Immunity *21*, 315–329.

Vicente-Manzanares, M., Choi, C.K., and Horwitz, A.R. (2009). Integrins in cell migration—the actin connection. J. Cell Sci. *122*, 199–206.

Wedlich-Soldner, R., and Li, R. (2003). Spontaneous cell polarization: undermining determinism. Nat. Cell Biol. *5*, 267–270.

Wilson, R.W., Ballantyne, C.M., Smith, C.W., Montgomery, C., Bradley, A., O'Brien, W.E., and Beaudet, A.L. (1993). Gene targeting yields a CD18-mutant mouse for study of inflammation. J. Immunol. *151*, 1571–1578.

Woolf, E., Grigorova, I., Sagiv, A., Grabovsky, V., Feigelson, S.W., Shulman, Z., Hartmann, T., Sixt, M., Cyster, J.G., and Alon, R. (2007). Lymph node chemokines promote sustained T lymphocyte motility without triggering stable integrin adhesiveness in the absence of shear forces. Nat. Immunol. *8*, 1076–1085.

Worbs, T., Mempel, T.R., Bölter, J., von Andrian, U.H., and Förster, R. (2007). CCR7 ligands stimulate the intranodal motility of T lymphocytes in vivo. J. Exp. Med. *204*, 489–495.

Wu, M.T., and Hwang, S.T. (2002). CXCR5-transduced bone marrow-derived dendritic cells traffic to B cell zones of lymph nodes and modify antigen-specific immune responses. J. Immunol. *168*, 5096–5102.